Graphical Abstract

Predicting paint resistance to pull-off by first principles calculations: the case of acrylic acid on (oxidised) metals

Manuel Montebelli, Paolo Restuccia, M. Clelia Righi

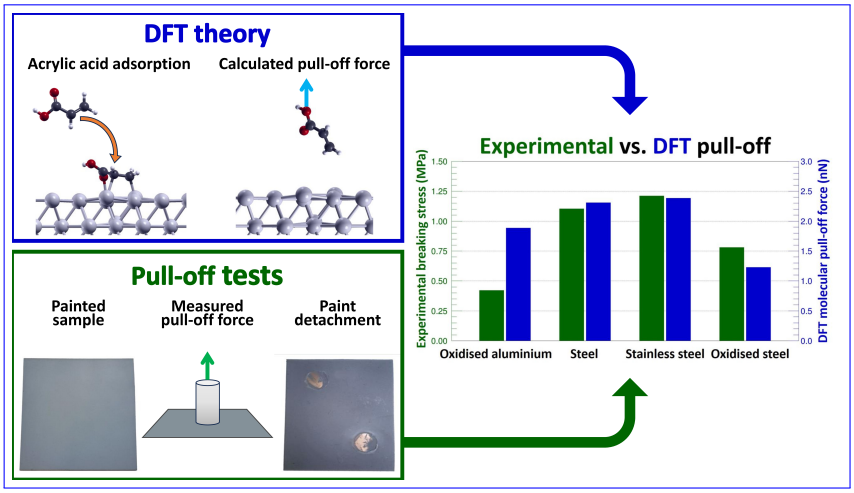

Highlights

Predicting paint resistance to pull-off by first principles calculations: the case of acrylic acid on (oxidised) metals

Manuel Montebelli, Paolo Restuccia, M. Clelia Righi

- DFT ~~simulations matched experimental trendsranking adhesion strength across substrates~~ pull-off forces reproduce experimental trends: DFT used to predict paint adhesion
- Substrate oxidation ~~significantly reduced acrylic acid adhesion and pull-off forces~~ weakens acrylic acid binding, reducing adhesion
- ~~Acrylic acid adhesion on steel promoted by the interaction with surface C and Cr~~ Highest adhesion on stainless-steel due to molecule interaction with Cr and C atoms

Predicting paint resistance to pull-off by first principles calculations: the case of acrylic acid on (oxidised) metals

Manuel Montebelli[a], Paolo Restuccia[a,*], M. Clelia Righi[a,*]

[a]*Dipartimento di Fisica e Astronomia, Università di Bologna, Viale Berti Pichat 6/2, Bologna, 40127, Italy*

Abstract

Paints are essential in everyday applications ~~, providing~~ since they provide protective functions beyond aesthetics, such as corrosion resistance, UV shielding, and thermal performance enhancement. ~~However, the effectiveness of these properties heavily depends on paint adhesion to substrates. While empirical tests evaluate adhesion strength and durability, an atomistic insight is highly desirable for optimising paint-substrate interactions. This work proposes a predictive computational method based on Density Functional Theory to predict the pull-off resistance of acrylic paint. Molecule-substrate interactions at the nanoscale were modelled to study~~ Adhesion is a critical factor governing the durability and performance of paints, yet the mechanisms controlling it at the atomic scale remain poorly understood. Here, we show that density functional theory (DFT) calculations can complement empirical adhesion tests and support the rational design of paint–substrate systems. We considered acrylic acid

*Corresponding authors

Email addresses: paolo.restuccia@unibo.it (Paolo Restuccia), clelia.righi@unibo.it (M. Clelia Righi)

(a key component of acrylic paint) on pure and oxidised ~~metals, namely~~ metallic substrates, including aluminium, iron, steel, alumina, hematite and goethite. ~~Adsorption energies were calculated and experimental~~ The calculated adsorption energies and pull-off ~~tests were subsequently mimicked~~forces were compared with experimental paint breaking stress. The results ~~indicated that the paint attaches more strongly on~~ show that acrylic acid binds more strongly to pristine metals than ~~oxides, aligning with literature and macroscopic experimental tests performed in laboratories. Simulations matched experimental trends accurately ranking adhesion strength across substrates. These findings highlighted the predictive power of the adopted computational approach, paving the way for a computational design of paint-substrate pairs with tailored properties~~to oxides, and more in general the trends obtained across the considered substrates were in excellent agreement with the experiments, thereby establishing a quantitative correlation between molecular adsorption and macroscopic paint scratch. This approach offers a transferable route to design tailored coating–substrate systems, supporting applications in substrate protection and durability.

Keywords:
acrylic acid, paint adhesion, molecular adsorption, density functional theory, pull-off experiments

---

1. Introduction

Painting has been part of the history of humankind since the Stone Age: the first archaeological evidence of painting practices by Homo Sapiens dated

back 100,000 years [1]. Nowadays, paints and coatings play a pivotal role far beyond artistic and aesthetic applications, being ubiquitous in many industrial sectors. For example, in the automotive field, paints are applied on the car body not only for aesthetic purposes but also for resistance to weather, scratch and environmental agents [2]. The global business of paints and coatings reached 180 billion U.S. dollars in 2023 [3].

Among the different types of paints available on the market, acrylic paints are one of the most commonly used thanks to their excellent adhesion properties on different substrates [4, 5][4–6]. Their fundamental components are acrylic resins, which consist of a mixture of copolymers, like poly(methyl-methacrylate), poly(ethyl-acrylate), and poly(n-butyl-acrylate), with all of them containing an O−C=O functional group coming from their primary constituent, namely acrylic acid (CH_2=CHCOOH) [7]. These chemical compounds are responsible for the key properties that led acrylic paints to success: fast drying times, solubility in water, and applicability to different surfaces.

As evident, the adhesion of paints and coatings to the underlying substrate directly influences their performance and effectiveness. It is paramount to evaluate how well a paint remains attached under mechanical or environmental stress. At the atomistic level, the resistance to peel-off arises from the molecular adsorption of paint constituents onto the substrate, a process that ultimately governs the paint's durability and resistance to delamination [8, 9][8–10]. In the case of acrylic paints, the reactivity of the acrylates and methacrylates present in the solution leads to the strong adhesion of such paints on different substrates, like metals, glass and plastics like PVC [5].

Over the years, numerous techniques were developed to evaluate the paint adhesion on a substrate. Among these, mechanical tests determining the stiffness, toughness and likelihood of cracks at the paint-substrate interface play a key role in assessing its lifetime stability [11]. Different types of machinery can be employed for these tests. The pull-off test, as described in ISO 4624 [12], comprises a simple instrumentation allowing an immediate evaluation of the adhesion strength, whereas the double cantilever beam test ~~[13]~~ [13, 14] provides a more detailed characterisation of adhesion, but requires more time at higher costs. Additionally, peel and shear tests are usually employed to assess adhesion properties, providing quantitative measures of bond strength and reveal different failure modes at the interface [15]. Peel tests evaluate the force required to separate bonded layers by peeling, while shear tests measure the adhesive's resistance to forces applied parallel to the interface, simulating real-world loading conditions. Nonetheless, these experimental methods measure macroscopic adhesion without revealing the molecular-scale mechanisms that govern adhesion energy, nor do they offer predictive insight into whether a paint will adhere strongly or weakly on a given substrate. Establishing an accurate molecular-level understanding is paramount to define the direct correlations between interfacial atomic configurations and adhesion properties, thereby creating a rational basis for the design of coating–substrate systems with improved performance.

Computational methods, particularly those based on density functional theory (DFT), help bridge this gap by quantifying the resistance to detachment of a coating or a paint from its substrate. In the case of solid coatings, the interfacial adhesion energy, which is the opposite of the work per

unit area required to separate two solid surfaces from contact, provides a quantitative measure of bonding strength between the coating surface and substrate surface. This quantity is directly related to the surface energies of the two solids [16, 17]. In the case of paints, composed by single molecules, the microscopic quantity that determines the adhesive strength is the molecular adsorption energy. In DFT calculations both the interfacial adhesion energy and the molecular adsorption energy can be accurately estimated as the difference between the energy of the compound and the energies of the separated constituents, e.g.,

$$E_{\text{adhesion/adsorption}} = E_{12} - E_1 - E_2 \tag{1}$$

where E_1 is the energy of the isolated molecule (coating), E_2 the energy of the clean substrate, and E_{12} the energy of the molecule (coating) on the substrate. Atomistic simulations can constitute powerful predicting tools capable of capturing the physico-chemical interactions that underpin material behaviour across a range of fields, including catalysis [18], energy storage [19], corrosion [20], microelectromechanical systems [21], and tribology [22]. Recent studies on mineral-polymer and metal-polymer interfaces underscore the effectiveness of combining experimental and computational approaches to unravel adhesion mechanisms. For example, DFT calculations of wollastonite (a calcium silicate mineral) adsorption on cellulose and hemicellulose revealed that hydrogen bonding and electrostatic interactions govern adhesion energy, with theoretical adsorption distances (1.5–2.0 Å) aligning closely with X-ray diffraction data [23–25]. In this context, DFT is not only a diagnostic tool, but can be used as a framework for designing materials: by

linking interfacial atomic configuration and chemistry to adhesion properties, it predicts how surface modifications such as surface oxidation or alloying affect coating performance. This connection is central to developing coatings with targeted durability and functionality.

In the context of paint adhesion, most DFT studies have focused on epoxy resins, investigating their interaction with various substrates, including phosphates [26], metals [27] and protective oxidative layers on steel [28]. These works have clarified how atomic-scale interactions influence adsorption mechanisms in epoxy-based coatings. In contrast, atomistic studies on acrylic paints remain significantly less developed, with only ~~a~~ few *ab initio* investigations focused on adsorption on specific substrates such as rutile [29]. Complementary molecular dynamics simulations have examined the effect of environmental pollutants on acrylic polymers, offering insights into their degradation mechanisms [30].

In this work, we extended the knowledge of acrylic paint adhesion by showing how computational and experimental approaches can be combined to evaluate this process on various metallic and oxidised substrates. DFT simulations were performed by considering the functional monomer of acrylic paints, i.e., *acrylic acid*, adsorbed over different substrates, namely Al(111), Fe(110), C@Fe(110), Cr@Fe(110), Ni@Fe(110), α-Al_2O_3(0001), α-Fe_2O_3(0001) and α-FeO(OH)(100). We computed the molecular adsorption energies and pull-off forces, comparing them with pull-off tests performed at the Istituto Giordano laboratories (Italy), where a tensile stress was applied to a paint-substrate system to record its detachment stress. The excellent agreement of DFT data with the experimental trends proved the predictive

power of *ab initio* simulations in studying paint adhesion. By explicitly correlating the molecular adsorption configuration, the adhesion strength, and the substrate oxidation, our study demonstrates how simulations can proactively guide the design of coating–substrate systems with tailored performance for protection and durability.

2. Methods

2.1. Computational methods

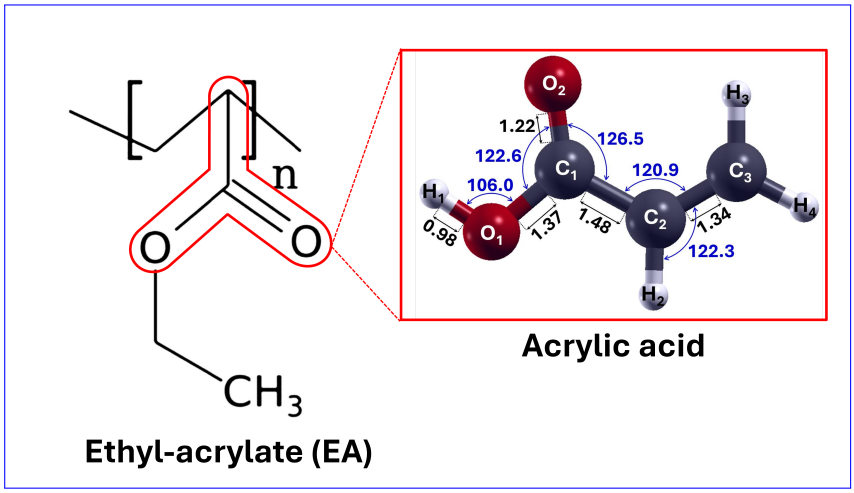

Figure 1: Molecular structure of ethyl-acrylate (EA), an an acrylic binder (left). Its functional unit, marked in red, origins from acrylic acid (ball-and-stick representation on the right). Relevant bond lengths (in Å, black colour) and angles (in °, blue colour) of acrylic acid molecule calculated after the DFT structural optimization are shown.

Usually, acrylic paints formulation is very complex, consisting of a solvent, a binder, pigments and additives carefully selected to meet the specific requirements of their intended applications. In particular, binders are a mixture of long, branched chain of acrylic polymers descending from the same

monomer, namely the acrylic acid (ball-and-stick representation in Fig. 1 inset). This molecule constitutes the functional group of all binder polymers, which are constructed from it by adding a methyl group or a longer hydro-carbon chain at its head and tail. Therefore, the acrylic acid molecule has been chosen as representative of the reactive components as also done in previous studies [29–32].

The DFT simulations were performed using the Quantum ESPRESSO suite [33] and the exchange and correlation functionals were estimated within the generalised gradient approximation, adopting the PBE functional [34] in a spin-polarized setup. All the substrates under study were modelled with a slab geometry. Each slab was placed in a supercell of suitable height (at least 15 Å of vacuum space above the topmost atomic layer) to avoid interaction with replicas along the z direction. The simulations cells and computational parameters were independently optimised for each system, starting from their elemental bulks. In particular, the lattice parameters were determined by fitting the energy-volume data to the Birch–Murnaghan equation of state [35]. This procedure was also used to determine the convergence cut-off for the plane wave expansion. In addition, the **k**-point sampling, based on a Monkhorst-Pack grid [36], was also optimised at the bulk level. Supercells for surface calculations were then constructed by rescaling and adapting the cell parameters obtained from the bulk optimisations, ensuring consistency across all simulations. Specifically, the aluminium had a lattice parameter of 4.046 Å, with an Al(111) orthorhombic supercell with an in-plane size of 14.87 Å × 8.58 Å. For iron, the lattice constant was 2.85 Å, with Fe(110)-based orthorhombic supercells of 14.19 Å × 12.04 Å in-

plane area. The $Al_2O_3(0001)$ hexagonal supercell had lateral lattice parameter $a = 4.81\,\text{Å}$, with a 2×2 in-plane size for the employed supercell. The α-Fe_2O_3 unit cell was $5.105\,\text{Å} \times 4.42\,\text{Å}$, with an orthorhombic supercell of $10.21\,\text{Å} \times 8.84\,\text{Å}$ in-plane size. Finally, the α-FeO(OH) orthorhombic unit cell was $3.05\,\text{Å} \times 4.54\,\text{Å}$, with a resulting 5×3 supercell of $15.24\,\text{Å} \times 13.63\,\text{Å}$. A 40 Ry energy cut-off for the plane-waves was employed in the Al(111) and Fe(110) substrates, whereas $Al_2O_3(0001)$, $Fe_2O_3(0001)$ and FeO(OH)(100) had a 50 Ry energy cut-off. The optimal sampling for the Al(111), $Fe_2O_3(0001)$ and FeO(OH)(100) substrates was at the $\mathbf{\Gamma}$-point, whereas Fe(110) and $Al_2O_3(0001)$ had an optimal sampling in a $(2 \times 2 \times 1)$ $\mathbf{k}$-points grid. The $Fe_2O_3(0001)$ and FeO(OH)(100) slabs were simulated using the DFT+U formalism, applying the Hubbard U term on the 3d manifold of Fe by setting $U = 4.2\,\text{eV}$ [37]. Moreover, an initial antiferromagnetic magnetization for the valence electrons of these substrates was set to represent the antiferromagnetic character of hematite and goethite [38, 39].

To model the stainless steel employed in the experiments, three configurations were created, referred to as C@Fe(110), Cr@Fe(110) and Ni@Fe(110). These surfaces incorporated common elements present in stainless steel, namely carbon, chromium and nickel, into the Fe(110) substrate. In this way, the atomistic effect of such dopants in the adsorption of acrylic acid could be evaluated. For each of the steel-like substrates, the formation energy of the alloy ΔE_{alloy} was calculated to understand whether their formation was endothermic or exothermic. For C@Fe(110) slab, where an interstitial C atom was included at the surface, ΔE_{alloy} was calculated as:

$$\Delta E_{\text{alloy}} = E_{\text{DS}}^{(N+1)} - \left(E_{\text{FeS}}^{(N)} + E_{\text{DB}}^{(1)}\right) \tag{2}$$

while for Cr@Fe(110) and Ni@Fe(110) slabs, where the dopants substituted a surface Fe atom, ΔE_{alloy} was calculated as:

$$\Delta E_{\text{alloy}} = \left(E_{\text{DS}}^{(N)} + E_{\text{FeB}}^{(1)}\right) - \left(E_{\text{FeS}}^{(N)} + E_{\text{DB}}^{(1)}\right) \tag{3}$$

where E_{DS} is the energy of the relaxed steel-like slab, E_{FeS} is the energy of the relaxed iron slab, E_{DB} is the energy of a dopant atom placed in its native bulk and E_{FeB} is the energy of an iron atom placed in its native bulk. The superscripts in brackets indicate the number of atoms of the system corresponding to the underlying energy value. E_{DS} values were calculated with the same computational settings adopted for the pure iron slab. The ΔE_{alloy} values were negative in all the steel-like slabs (-0.01 eV, -0.17 eV and -0.42 eV for C@Fe(110), Cr@Fe(110) and Ni@Fe(110), respectively) indicating that the formation of these alloys is an exothermic process and suggesting that substitution (or addition) of these elements into the iron bulk is a favourable process.

The surface energy E_{surf} of all the slabs was calculated according to the following formula:

$$E_{\text{surf}} = \frac{1}{2A}(E_{\text{slab}} - NE_{\text{bulk}}) \tag{4}$$

where E_{slab} is the total energy of the supercell containing the slab, N is the number of atoms in the slab, E_{bulk} is the energy per atom, A is the surface area, and the factor 2 is inserted when the slab has two equivalent surfaces. In the steel-like substrates, the two surfaces were not equivalent,

with the bottom one composed of pure iron. In this case, the energy of the doped surface $E^{\mathrm{sl}}_{\mathrm{surf}}$ was computed as:

$$E^{\mathrm{sl}}_{\mathrm{surf}} = \frac{1}{A}(E^{\mathrm{sl}}_{\mathrm{slab}} - E^{\mathrm{sl}}_{\mathrm{bulk}}) - E^{\mathrm{Fe}}_{\mathrm{surf}} \tag{5}$$

where $E^{\mathrm{sl}}_{\mathrm{slab}}$ is the energy of the steel-like slab, $E^{\mathrm{sl}}_{\mathrm{bulk}}$ is the energy of the steel-like bulk and $E^{\mathrm{Fe}}_{\mathrm{surf}}$ is the surface energy of the bottom pure iron surface.

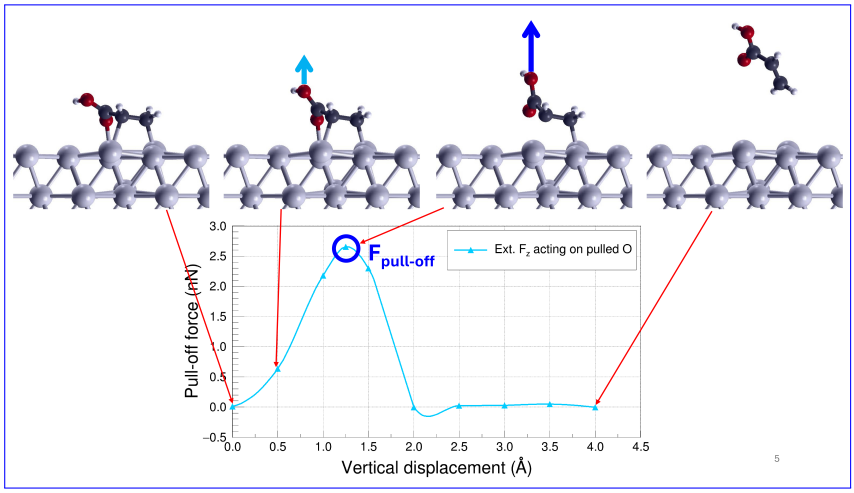

Figure 2: Example of a molecular pull-off procedure for acrylic acid over Al(111): the upper panel show some snapshots of the different molecule displacements. The graph in the lower panel reports the force variation during the displacement of the molecule. The highest value of the force (circled in blue) is the pull-off force $F_{\text{pull-off}}$

To compute the molecular adsorption of acrylic acid over the different substrates, we exploited the Xsorb software developed by our group [40], which allows an automatic search of the global minimum for molecular adsorption. It employs Python libraries like ASE [41] and Pymatgen [42] to automatically explore the configurational space of molecular adsorption. First, it performs a preliminary optimisation to pick out the most probable adsorption arrange-

ments, then it fully optimises these configurations with tighter convergence thresholds to identify the adsorption minimum. In this final configuration, Xsorb computes the adsorption energy E_{ads} as:

$$E_{\mathrm{ads}} = E_{\mathrm{surf+mol}} - (E_{\mathrm{surf}} + E_{\mathrm{mol}}) \tag{6}$$

where $E_{\mathrm{surf+mol}}$ is the energy of the molecule adsorbed over a slab, while E_{surf} (E_{mol}) is the energy of the isolated substrate (molecule). With this definition, $E_{\mathrm{ads}} < 0$ means that adsorption is an exothermic (thus spontaneous) process.

Once the optimal adsorption configuration for each molecule-substrate combination is determined, molecular pull-off processes were simulated by implementing a method previously adopted in Ref. [43]. For each system, the pull-off was performed by increasing the z-coordinate of a selected atom of the molecule by $\Delta z = 0.5\,\text{Å}$, followed by a system relaxation. This procedure was repeated on the output system in an iterative cycle until the molecule was detached from the substrate. Two pull-off simulations were performed for each substrate by displacing both the protonated oxygen bound to the carbon chain and the carbon of the apical CH_2 group, respectively (O_1 and C_3 according to Fig. 1). Each system was optimised by keeping fixed the z-coordinate of the pulled atom and all atomic coordinates of the slabs to eliminate possible substrate deformations. The residual force on the pulled atom represented the force necessary to keep the atom at the fixed distance from the surface, and it is thus assumed as the pull force F_z. In this way, it is possible to evaluate only the force necessary to break the chemical bonds between the molecule and the substrate. In general terms, F_z vs. Δz curves

show one or more peaks at the breaking points of chemical bonds, followed by an asymptotic tendency to zero once the molecule was detached from the substrate. The pull-off force $F_{\text{pull-off}}$ of the system was identified as the highest peak. A schematic representation of this procedure is shown in Fig. 2.

2.2. Experimental methods

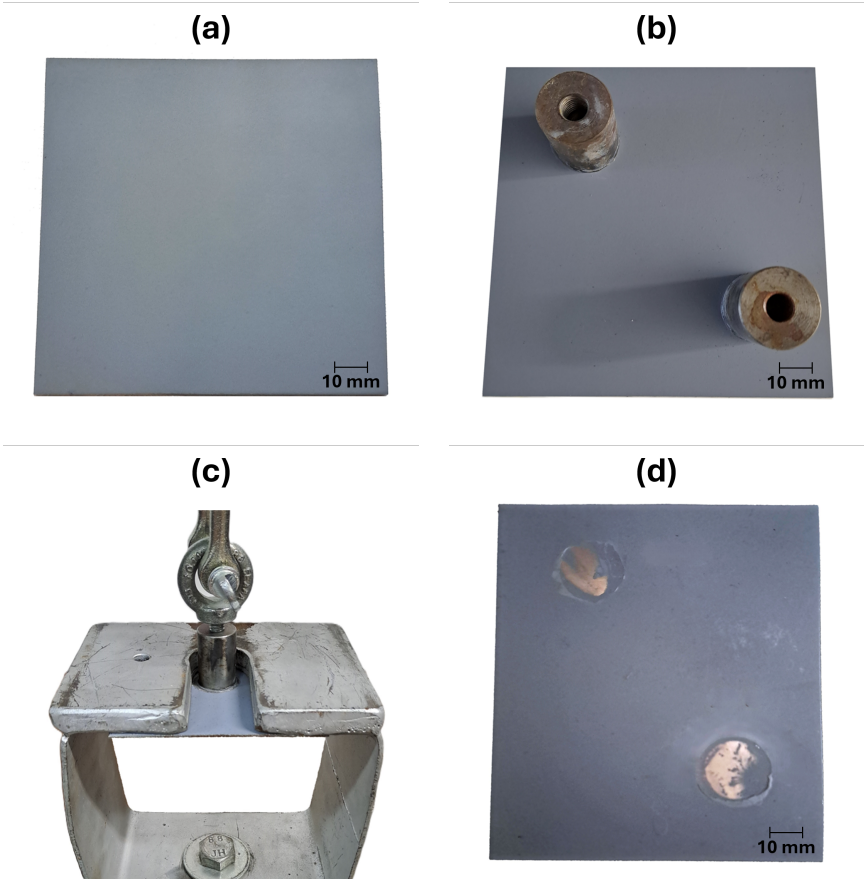

Figure 3: Schematic representation of the experimental procedure. (a) The sample was coated with acrylic paint. (b) The painted sample had two dollies glued onto its surface. (c) The sample was put in the pull-off tester. (d) The sample is analysed after the test.

Pull-off tests were performed on painted samples to link the macroscopic detachment stress measurable experimentally to the DFT pull-off forces. The tests were carried out at the Istituto Giordano laboratories in Bellaria-Igea Marina (Italy) according to the standard ISO 4624 method B [12]. Flat 100 mm × 100 mm samples consisting of different materials, namely aluminium, S235JRG2 steel, AISI 304 stainless steel, and oxidised S235JRG2 steel, were employed, each coated with an acrylic paint.

S235JRG2 steel had a nominal C content of ≤ 0.17 wt.%, while AISI 304 stainless steel had a C content ≤ 0.07 wt.%, Cr content 17.5 - 19.5 wt.%, Ni content 8.0 - 10.5 wt.%. The oxidised steel samples were obtained from non-oxidised ones by first exposing them to a corrosive atmosphere containing water vapour and sulphur dioxide for 2 hours: they were placed in a 300 dm^3 humidistat chamber loaded with 2 dm^3 of water with electrical conductivity $\kappa \leq 500\,\mu\mathrm{S/m}$ heated to 40 °C to create a water vapour-saturated atmosphere. Next, a corrosive sulphuric acid atmosphere was created by pumping 0.2 dm^3 of sulphur dioxide gas into the chamber. After washing the samples with water to eliminate acid surface residuals, they were exposed to a 80 °C and 80 %RH atmosphere in a climatic chamber for 48 hours to complete the oxidation process.

Once the samples were cleaned to remove surface residues, they were painted with an acrylic-based paint for which the producer declared good adhesion properties both on clean and rusted metal surfaces. According to its datasheet, the paint was composed of 24 wt.% P(MMA-co-nBA) acrylic resin as binder, 68 wt.% organic solvent, composed of acetone and xylene, and 8 wt.% grey pigment and additives. The paint was applied on the sam-

ples at 20 °C and left to dry under room conditions for 120 hours prior to testing. Close attention was paid to depositing the paint homogeneously on the samples to ensure a uniform and full coverage of the substrate surface. A painted sample is shown in Fig. 3a.

The pull-off test was carried out on 2 test areas for each sample by placing them in a computer-controlled electronic tensile tester, which applied the tensile stress. It was equipped with a load cell to record the applied force. The tensile stress was obtained by normalising this force to the test area. The latter were set up by gluing two steel cylinders with 20 mm diameter and threaded head, called dollies, onto each sample (see Fig. 3b). Ethyl-cyanoacrylate glue by Henkel was used. Testing was conducted 168 after gluing to ensure complete curing of the adhesive. Once the samples were prepared, they were placed in the sample holder of the tensile tester, which was shaped to align the dolly coaxially to the tester moving end during traction. One dolly at the time was screwed to the moving end of the tester, which had a lifting speed of 8 mm/min. This velocity was chosen to achieve a pressure rate of 0.33 MPa/s, which is below the maximum value of 1 MPa/s prescribed by the ISO 4624 standard, and within the same order of magnitude as loading speeds reported in the literature [44]. This procedure gradually increased the applied stress until the dolly was detached from the sample (Fig. 3c). The maximum force detected, corresponding to detachment of the dolly, was the pull-off force of the tested paint area. It was normalized to the test area $A \approx 314\,\mathrm{mm}^2$ to obtain a dolly surface-independent breaking stress σ, expressed in megapascals. This procedure was repeated on all samples, averaging the results obtained for each substrate. One sample after test is

shown in Fig. 3d.

3. Results

3.1. Computational results

We started our study by placing the acrylic acid in a 20 Å × 20 Å × 20 Å supercell and optimising its structure. The optimal molecular geometry was planar, and its bond lengths and angles, reported in both the inset of Fig. 1 and Table S1 of the Supplementary Materials, were in agreement with the literature [45].

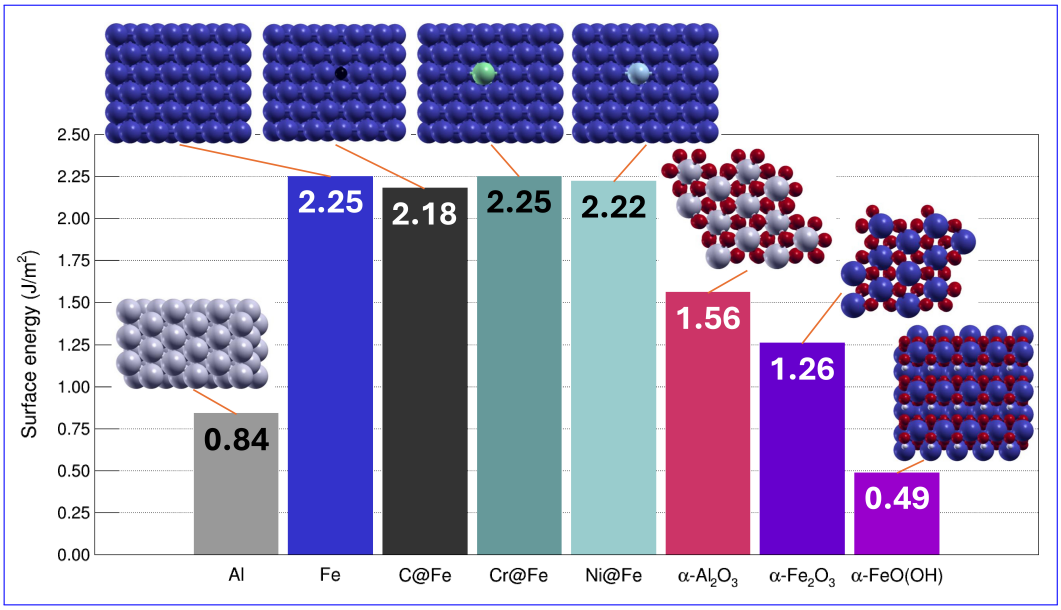

Figure 4: Surface energy values (in J/m^2) and atomistic representation of the considered substrates: Al(111) (grey), Fe(110) (navy), C@Fe(110) (dark gray), Cr@Fe(110) (teal), Ni@Fe(110) (light blue), Al_2O_3(0001) (magenta), Fe_2O_3(0001) (indigo) and FeO(OH)(100) (purple).

The surface energies for all the substrates under examination were computed, and the reported values in Fig. 4 were usually proportional to the reactivity of the corresponding surface, providing a preliminary information about its tendency to molecular adsorption. It is immediate to notice that Fe(110) and the steel-like substrates have the highest surface energies, around 2.2 J/m^2, confirming the high reactivity of iron substrates due to their partially occupied 3d orbitals. It is also evident the E_{surf} reduction caused by iron oxidation, which is even more evident for the hydroxylated surface of goethite where the surface energy is reduced almost by a factor 5. On the contrary, oxidation increases the surface energy of aluminium: α-Al_2O_3 is a strongly ionic oxide and its reconstructed surface termination is unstable, since it leaves bare surface Al^{3+} ions or dangling O-bonds.

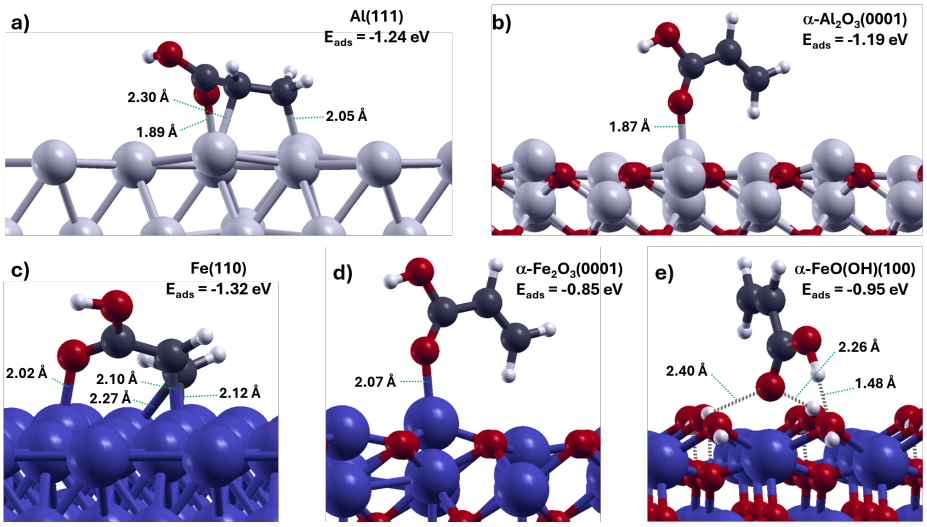

Figure 5: Side views of the most stable adsorption configurations for acrylic acid onto Al(111) (panel a), Al_2O_3(0001) (b), Fe(110) (c), Fe_2O_3(0001) (d) and FeO(OH)(100) (e) substrates. The values for E_{ads} are reported as insets.

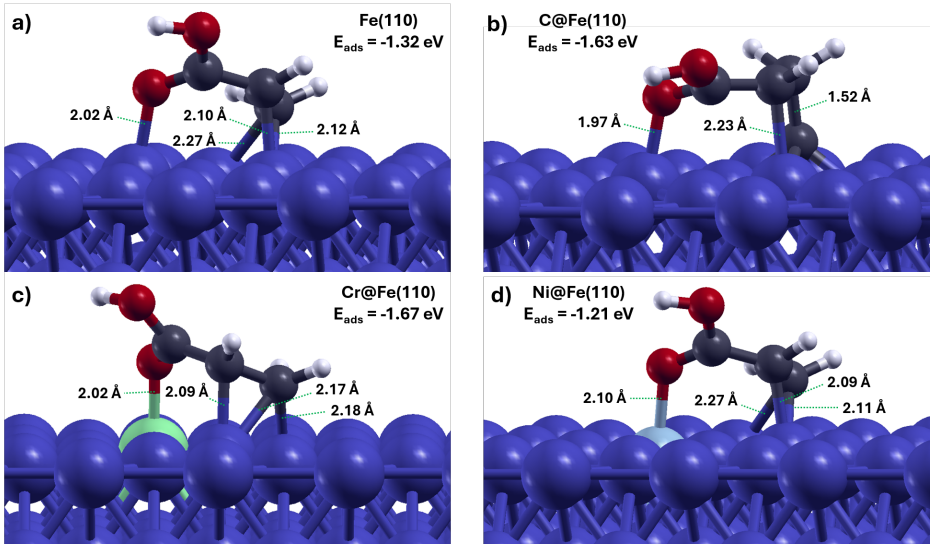

Figure 6: Side views of the most stable adsorption configurations for acrylic acid onto Fe(110) (panel a), C@Fe(110) (b), Cr@Fe(110) (c), and Ni@Fe(110) (d) substrates. The values for E_{ads} are reported as insets.

Then, the optimal adsorption configuration for all molecule-substrate combinations was found with Xsorb and their adsorption energies E_{ads} were computed, which are reported in Figs. 5-6. The data suggested the good adhesion properties of acrylic acid on both clean and oxidised substrates, with adsorption energies in the order of the electronvolt, comparable to other organic molecules [46–49]. It is immediate to notice two general trends for acrylic acid adsorption depending on the nature of the substrate. The adsorption energies reduced significantly on oxidised substrates (Fig. 5), especially on iron oxides. On the other hand, the steel-like substrates C@Fe and Cr@Fe (Fig. 6) enhanced the reactive character of the iron substrates thanks to the acrylic acid interaction with the C and Cr dopants. The pictorial representations of the most stable adsorption configurations in Figs. 5-6 pro-

vide further evidence of these results. Over metallic surfaces, the acrylic acid molecule settled planar to the surface, whereas for the oxidised substrates the molecular plane was orthogonal to the surface. This qualitative consideration suggests a better adhesion on clean metals, supporting the quantitative results. The observed difference in adsorption configuration arises because, on metallic substrates, both the head and the tail groups of the molecule interact with the substrate, whereas oxidised substrates show stronger affinity for the head group and a weaker interaction with the tail of acrylic acid. Indeed, molecules terminating with a carboxylic group often interact with an oxidised substrate through the carbonyl oxygen [50–52], while also forming long-range hydrogen bonds via the hydroxyl group, as observed in the case of goethite. In addition, the electronic structure of the substrates plays a significant role in determining the adsorption geometry. Metallic surfaces, with their delocalised electrons, enable extended interactions with the adsorbate, thereby increasing the adsorption energy. In contrast, oxide surfaces promote more directional covalent bonding, typically involving fewer atoms. This distinction contributes to the observed variation in adsorption configurations between metallic and oxidised substrates.

The optimal adsorption configuration for each molecule-substrate combination was the starting point for the calculation of the molecular pull-off forces $F_{\text{pull-off}}$, as explained in Section 2.1. The numerical values are reported in the histogram plot shown in Fig. 7, while the force against vertical distance plots for all molecule-substrate systems are shown in the Supplementary Materials in Figs. S1a-h.

From evaluating $F_{\text{pull-off}}$, it is possible to notice again that oxidation re-

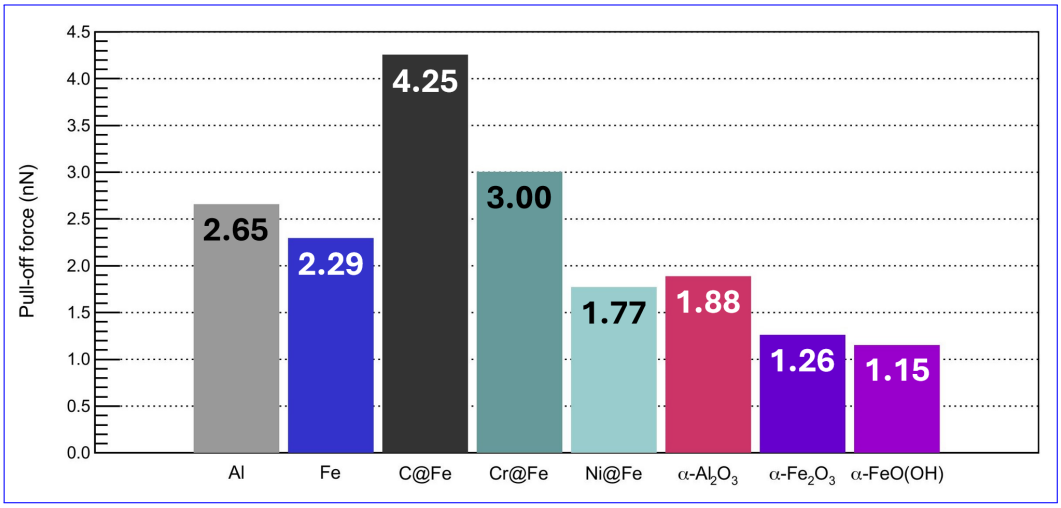

Figure 7: Molecular pull-off force $F_{\text{pull-off}}$ (nN) of the considered substrates: Al(111) (grey), Fe(110) (navy), C@Fe(110) (dark gray), Cr@Fe(110) (teal), Ni@Fe(110) (light blue), Al_2O_3(0001) (magenta), Fe_2O_3(0001) (indigo) and FeO(OH)(100) (purple).

duces the resistance to pull-off of acrylic acid, which is consistent to the adsorption calculations. For aluminium, $F_{\text{pull-off}}$ decrease by 29%. For iron, it dropped by 45% (50%) when considering hematite (goethite) as the oxidised substrate. In general, similar trends for molecular adsorption energies and molecular pull-off force values have been found, as expected. In particular, the C@Fe(110) substrate was the one with the highest value of $F_{\text{pull-off}}$, at 4.25 nN, due to the strong interaction of the covalent C−C bond. This large interaction was also evident by the shape of the force peak in Fig. S1c of the Supplemental Materials, which was extremely narrow and with a sharper decrease to zero compared to the other systems. This trend of $F_{\text{pull-off}}$ was associated with an immediate cancellation of the charge transfer on the C−C bond after the force peak, as shown in Fig. S2. This insights confirmed the presence of a strong covalent bond extremely difficult to break when the

acrylic acid interacted with a C atom of the steel substrates.

3.2. Pull-off experiments

As mentioned in Section 2.2, the experimental breaking stress was calculated for each substrate by averaging the values measured on each test area. The results for the breaking stresses σ are shown in Fig. 8a alongside the weighted averages of the DFT pull-off forces (Fig. 8b), whose values are taken from Fig. 7. For the calculation of the DFT forces, the concentrations of the elements present in the experimental substrates were employed as weights (neglecting minor dopants not included in the present study), using the formula $F_{\text{pull-off}} = \sum w_i F_{\text{pull-off},i}$. In particular, the assumed mass composition for steel was 99.83 wt.% Fe, and 0.17 wt.% C@Fe, stainless steel had a weight concentration of 71.93 wt.% Fe, 0.07 wt.% C@Fe, 18.0 wt.% Cr@Fe, and 10.0 wt.% Ni@Fe, and for oxidised steel the assumed molecular composition was 50.0% α-Fe_2O_3 and 50.0% α-FeO(OH). Bare aluminium surfaces are well known to quickly oxidise when exposed to standard environmental conditions, therefore they were considered completely oxidised with a 100 wt.% composition of α-Al_2O_3. At first glance, it is clear the trends of the experimental and theoretical data were in good agreement, especially for steel and stainless steel, whereas the major difference arose from the aluminium substrate. The experimental trend in breaking stress, showing stronger adhesion for metallic substrates compared to oxides, was also supported by the visual assessment method outlined in ISO 4624, which allowed to evaluate the fracture types during dolly detachment, described in detail in the Supplementary Materials. The results in section S4 of the Supplementary Materials clearly indicate that adhesive failure between the substrate and paint, where the

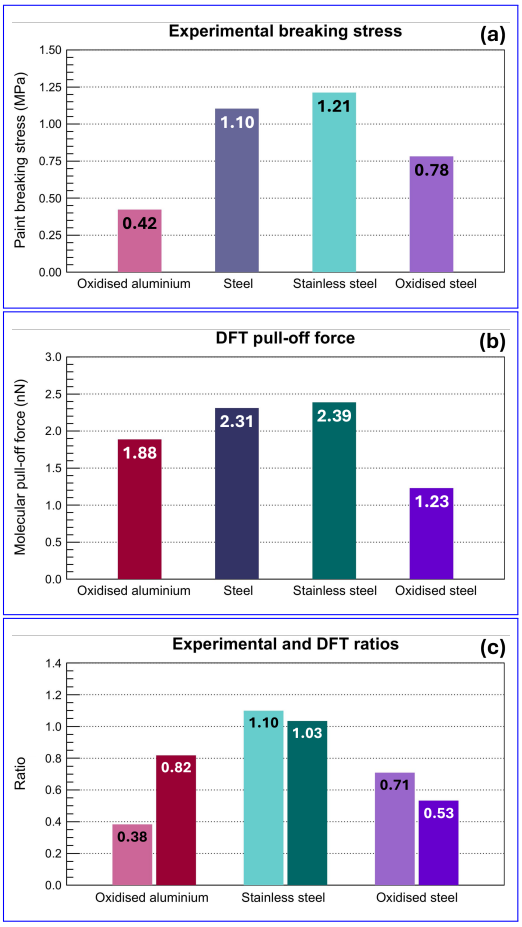

Figure 8: (a) Breaking stresses σ (in MPa) to detach acrylic paint from oxidised aluminium, S235JRG2 steel, AISI 304 stainless steel, oxidised S235JRG2 steel samples. (b) Average value for the molecular pull-off obtained in DFT simulations considering the weight composition of the experimental samples. (c) Comparison between the experimental σ_{ratio} (lighter colours) and theoretical F_{ratio} (darker colours), both normalised to the values for steel, which was taken as the reference substrate.

paint fully detaches from the substrate and remains on the dolly, was more frequent for oxidised surfaces than for metallic ones. This kind of failure generally indicates that paint-substrate adhesion is weaker than in systems where cohesive failure of the same kind of paint occurs, meaning that the paint splits with part remaining attached to the substrate and part to the dolly. In our experiment, cohesive failures were more common on metallic surfaces, suggesting stronger paint adhesion compared to oxidised ones. This observation aligns with both the pull-off test data and the DFT simulations.

A more quantitative comparison between theory and experiments can be achieved by normalizing both σ and $F_{\text{pull-off}}$ relative to the values obtained for steel, which was taken as the reference substrate. This normalization yields the quantities σ_{ratio} and F_{ratio}. As shown in Fig. 8c, an excellent agreement between theory for stainless steel was found, with discrepancies below 10%. The fact that both ratios exceed 1 suggests that the addition of chromium enhances steel adhesion properties, as anticipated by the DFT simulations.

The largest quantitative differences between σ_{ratio} and F_{ratio} arose when comparing oxidized substrates. In fact, the experimental adhesion strength for oxidized steel was higher than the theoretical prediction. On the contrary, the experimental adhesion for aluminium was significantly lower than both the theoretical value and the adhesion observed for all other substrates, leading to the most pronounced discrepancy. These deviations can be explained by surface roughness effects. Oxidized steel surfaces were rough and porous, features known to enhance paint adhesion, whereas the flat surfaces used in *ab initio* simulations lacked these characteristics. Smoother oxidized samples, produced via different oxidation techniques [48], may provide different

results and should be explored in future experiments.

Conversely, empirical comparisons with steel samples showed that aluminium surfaces were significantly smoother. Smooth surfaces are well known to hinder macroscopic adhesion by reducing the effective contact area available for bonding [53–55], which likely amplifies the observed experimental discrepancy between aluminium and steel. While the precise magnitude of this effect is difficult to quantify, different results may have been obtained using structured aluminium surfaces. In this study, we focused on testing the most common type of commercially available aluminium sheet to provide a relevant case study for practical applications. Future experiments should investigate the impact of structured aluminium surfaces on adhesion. It is worth noting that macroscopic adhesion can be also influenced by mechanisms like mechanical interlocking and physical adsorption, which were not explicitly included in our study. Our theoretical results showed adsorption energies on the order of electronvolts, which are substantially larger, by roughly an order of magnitude, than typical physical interactions [56], suggesting that chemical bonding is the dominant contribution in our systems. While mechanical interlocking involves many nanoasperities at length scales that are not captured by our DFT simulations, the agreement between our theoretical predictions and experimental results suggests that chemical adsorption provides a meaningful and representative contribution to the overall adhesion process.

In addition to these mechanisms, our computational model has further limitations that may influence the accuracy of the computed pull-off forces. The simulations assume atomically clean, flat surfaces and do not account for

solvent residues (e.g., water or organic co-solvents) that may remain trapped at the interface during paint adhesion. Experimental studies on acrylic adhesive films have shown that such residues can significantly hinder adhesion performance, indicating that solvent retention can alter adhesion kinetics in real paint interfaces [57]. Furthermore, our use of isolated acrylic acid molecules neglects the influence of polymer chains, including steric hindrance, chain-length dependence and cooperative effects which have been shown to affect surface coverage, wetting transition thresholds, and adsorption geometry in theoretical simulations [58–61]. While chemical bonding remains the dominant adhesion mechanism in our systems, consistent with the overall agreement between experimental and theoretical trends, these additional effects can partly explain the residual discrepancies.

In general, the employed substrates were representative of commercially available samples, in line with typical industrial practices where there is no routine characterisation of surfaces at the microscopic level. The excellent agreement between the macroscale experiments and DFT calculations, indicates that surface chemistry rather than surface morphology plays the major role in determining the paint resistance to pull off, consistently with the adhesive theory of friction proposed by Bowden and Tabor back in the fifties [62] and now well accepted in the tribology community.

4. Conclusions

This study ~~combined DFT simulations and experiments to investigate~~ introduced a DFT-based computational workflow to quantify the adhesion of acrylic paint on various metallic and oxidised substrates and validated the

results through comparison with pull-off experiments.

- Acrylic acid, the functional unit of acrylic polymers, was studied on eight substrates, including metallic (Al(111), Fe(110), C@Fe(110), Cr@Fe(110), Ni@Fe(110)), and oxidised surfaces (Al_2O_3(0001), Fe_2O_3(0001), and FeO(OH)(100)). Using Xsorb, ~~a software for the automatized study of molecular adsorption~~ software developed by our group [40] to automate the study of molecular adsorption, optimal adsorption configurations were identified, serving as input for pull-off simulations that quantified the molecular pull-off forces, i.e., the resistance to molecular detachment.

- The computational results showed stronger adhesion on metallic substrates, with steel-like ~~substrates~~surfaces, modelled as Cr@Fe(110) and C@Fe(110), exhibiting the highest adsorption energy and pull-off force, respectively. Oxidation consistently reduced adhesion, lowering pull-off forces by 29% for aluminium and up to 50% for iron. While overall trends between adsorption energies and pull-off forces were consistent, minor deviations revealed the complexity of molecular detachment mechanisms.

- The results of experimental pull-off tests on acrylic-coated substrates commonly used in industrial applications were in excellent agreement with the computational findings, showing deviations below 10% for metallic surfaces. Larger discrepancies on oxidised substrates, particularly aluminium, were attributed to differences in macroscopic surface properties, as the surface roughness.

~~These findings indicate that~~ Overall, these findings validated DFT-based ~~simulations can provide useful insights into paint adhesionand help the material design~~ modelling as a predictive framework for macroscopic coating adhesion. By linking adsorption configurations, adhesion strength, and substrate surface condition, our work demonstrated how computational insights can support the proactive design of coating-substrate systems. Future developments, including machine learning-based molecular dynamics to capture surface roughness and larger-scale effects ~~, could~~ (like the presence of environmental molecules), will further bridge the gap between theory and experiments~~in paint-substrate optimisation~~ , enabling the materials-by-design optimisation of durable protective coatings.

CRediT authorship contribution statement

Manuel Montebelli: Formal analysis, Investigation, Visualization, Writing – original draft. **Paolo Restuccia**: Formal analysis, Methodology, Writing – original draft, Writing – review & editing. **M. Clelia Righi**: Conceptualization, Funding acquisition, Supervision, Writing – review & editing.

Acknowledgements

We acknowledge the SLIDE project, which received funding from the European Research Council (ERC) under the European Union's Horizon 2020 research and innovation program. (Grant Agreement No. 865633). We also acknowledge the CINECA award under the ISCRA initiative, for the

availability of high-performance computing resources and support. We also want to thank Istituto Giordano for the access to its experimental facilities.

Data availability

Data will be made available on request.

References

[1] P. Akhter, A. Arshad, M. Hussain, A review on environmental impacts of paints and strategies for producing eco-friendly-paints, International Journal of Environmental Science and Technology (in press 2024). doi:10.1007/s13762-024-05760-z.
URL https://link.springer.com/article/10.1007/s13762-024-05760-z

[2] D. Mohanty, M. K. Kanny, S. Mohanty, S. K. Nayak, Characteristic properties of base coat of automobile paint: enhancement in scratch and abrasion resistance by nanoscale reinforcement - a review, Polymer Bulletin 80 (2023) 185–240. doi:10.1007/s00289-022-04081-w.
URL https://link.springer.com/article/10.1007/s00289-022-04081-w

[3] World's top ten paints companies 2023 annual report, Tech. rep., WPCIA (January 2024).
URL http://www.wpcia.org/news/World's%20Top%20ten%20Paints%20Companies%202023%20Annual%20Report.html

[4] F. N. Jones, W. Mao, P. D. Ziemer, F. Xiao, J. Hayes, M. Golden, Artist paints—an overview and preliminary studies of durability, Progress in Organic Coatings 52 (1) (2005) 9–20, conference on Coatings Science and Technology, Athens 2003. doi:10.1016/j.porgcoat.2004.03.008.
URL https://www.sciencedirect.com/science/article/pii/S0300944004001018

[5] F. Awaja, M. Gilbert, G. Kelly, B. Fox, P. J. Pigram, Adhesion of polymers, Progress in Polymer Science 34 (9) (2009) 948–968. doi:10.1016/j.progpolymsci.2009.04.007.
URL https://www.sciencedirect.com/science/article/pii/S0079670009000501

[6] L. Ecco, S. Rossi, M. Fedel, F. Deflorian, Color variation of electrophoretic styrene-acrylic paints under field and accelerated ultraviolet exposure, Materials & Design 116 (2017) 554–564. doi:10.1016/j.matdes.2016.12.051.
URL https://www.sciencedirect.com/science/article/pii/S0264127516315775

[7] T. Fardi, V. Pintus, E. Kampasakali, E. Pavlidou, M. Schreiner, G. Kyriacou, Analytical characterization of artist's paint systems based on emulsion polymers and synthetic organic pigments, Journal of Analytical and Applied Pyrolysis 135 (2018) 231–241. doi:10.1016/j.jaap.2018.09.001.
URL https://www.sciencedirect.com/science/article/pii/S0165237018304327

[8] K. L. Mittal, Adhesion measurement of thin films, Active and Passive Electronic Components 3 (1) (1976) 936912. doi:10.1155/APEC.3.21.
URL https://onlinelibrary.wiley.com/doi/abs/10.1155/APEC.3.21

[9] T. Utzig, S. Raman, M. Valtiner, Scaling from single molecule to macroscopic adhesion at polymer/metal interfaces, Langmuir 31 (9) (2015) 2722–2729. doi:10.1021/la504542f.
URL https://pubs.acs.org/doi/10.1021/la504542f

[10] H. Yang, C. Zou, X. Xu, M. Zang, S. Chen, Understanding of scratch behavior of an automotive coating system: Experiments and finite element analysis, Materials & Design 219 (2022) 110835. doi:10.1016/j.matdes.2022.110835.
URL https://www.sciencedirect.com/science/article/pii/S0264127522004579

[11] G. dePolo, M. Walton, K. Keune, K. Shull, After the paint has dried: a review of testing techniques for studying the mechanical properties of artists' paint, Heritage Science 9 (2021) 68. doi:10.1186/s40494-021-00529-w.
URL https://heritagesciencejournal.springeropen.com/articles/10.1186/s40494-021-00529-w

[12] Paints and varnishes - Pull-off test for adhesion, Standard, International Organization for Standardization (2023).
URL https://www.iso.org/standard/83350.html

[13] P. Ostojic, R. McPherson, Determining the critical strain energy release rate of plasma-sprayed coatings using a double-cantilever-beam technique, Journal of the American Ceramic Society 71 (10) (1988) 891–899. doi:10.1111/j.1151-2916.1988.tb07542.x.
URL https://ceramics.onlinelibrary.wiley.com/doi/abs/10.1111/j.1151-2916.1988.tb07542.x

[14] B. Z. Lu, Y. Qiao, E. K. Nickerson, Y. Shin, G. M. Schuler, N. L. Brown, N. L. Canfield, K. L. Simmons, Improving adhesive bonding of short carbon fiber thermoplastic composites to aluminum alloys with a hybrid laser-plasma surface modification strategy, Materials & Design 257 (2025) 114501. doi:10.1016/j.matdes.2025.114501.
URL https://www.sciencedirect.com/science/article/pii/S0264127525009219

[15] B. T. Poh, H. K. Kwo, Peel and shear strength of pressure-sensitive adhesives prepared from epoxidized natural rubber, Journal of Applied Polymer Science 105 (2) (2007) 680–684. doi:10.1002/app.26072.
URL https://onlinelibrary.wiley.com/doi/abs/10.1002/app.26072

[16] J. N. Israelachvili, Intermolecular and surface forces, Third Edition, Academic Press, 2011. doi:10.1016/B978-0-12-375182-9.10001-6.
URL https://www.sciencedirect.com/book/9780123751829/intermolecular-and-surface-forces

[17] P. Restuccia, G. Losi, O. Chehaimi, M. Marsili, M. C. Righi, High-throughput first-principles prediction of interfacial adhesion energies in

metal-on-metal contacts, ACS Applied Materials & Interfaces 15 (15) (2023) 19624–19633. doi:10.1021/acsami.3c00662.
URL https://pubs.acs.org/doi/full/10.1021/acsami.3c00662

[18] U. Diebold, The surface science of titanium dioxide, Surface Science Reports 48 (5) (2003) 53–229. doi:10.1016/S0167-5729(02)00100-0.
URL https://www.sciencedirect.com/science/article/pii/S0167572902001000

[19] L. Hu, J. W. Choi, Y. Yang, S. Jeong, F. L. Mantia, L.-F. Cui, Y. Cui, Highly conductive paper for energy-storage devices, Proceedings of the National Academy of Sciences 106 (51) (2009) 21490–21494. doi:10.1073/pnas.0908858106.
URL https://www.pnas.org/doi/abs/10.1073/pnas.0908858106

[20] K. Kousar, M. Walczak, T. Ljungdahl, A. Wetzel, H. Oskarsson, P. Restuccia, E. Ahmad, N. Harrison, R. Lindsay, Corrosion inhibition of carbon steel in hydrochloric acid: Elucidating the performance of an imidazoline-based surfactant, Corrosion Science 180 (2021) 109195. doi:10.1016/j.corsci.2020.109195.
URL https://www.sciencedirect.com/science/article/pii/S0010938X20324768

[21] R. Maboudian, R. T. Howe, Critical review: Adhesion in surface micromechanical structures, Journal of Vacuum Science & Technology B 15 (1) (1997) 1–20. doi:10.1116/1.589247.
URL https://pubs.aip.org/avs/jvb/article-abstract/15/1/1/470760/Critical-Review-Adhesion-in-surface

[22] A. Rosenkranz, B. Wang, D. Zambrano, J. Marqués Henríquez, J. Y. Aguilar-Hurtado, E. Marquis, P. Restuccia, B. C. Wyatt, M. C. Righi, B. Anasori, Solid-lubrication performance of $Ti_3C_2T_x$ - effect of tribo-chemistry and exfoliation, Materials Today Nano 25 (2024) 100464. doi:10.1016/j.mtnano.2024.100464.
URL https://www.sciencedirect.com/science/article/pii/S2588842024000142

[23] H. R. Taghiyari, J. Morrell, A. Husen, Emerging nanomaterials, Springer Cham, 2023. doi:doi.org/10.1007/978-3-031-17378-3.
URL https://link.springer.com/book/10.1007/978-3-031-17378-3

[24] H. R. Taghiyari, R. Majidi, A. Esmailpour, Y. S. Samadi, A. Jahangiri, A. N. Papadopoulos, Engineering composites made from wood and chicken feather bonded with uf resin fortified with wollastonite: A novel approach, Polymers 12 (4) (2020) 857. doi:10.3390/polym12040857.
URL https://www.mdpi.com/2073-4360/12/4/857

[25] H. R. Taghiyari, R. Majidi, S. M. Mohseni Armaki, M. Haghighatparast, Graphene as reinforcing filler in polyvinyl acetate resin, International Journal of Adhesion and Adhesives 113 (2022) 103075. doi:10.1016/j.ijadhadh.2021.103075.
URL https://www.sciencedirect.com/science/article/pii/S0143749621002785

[26] E. Sagvolden, M. F. Sunding, O. Swang, Surface reconstruction, hydration, and adhesion of epoxy to the (0001) surface of α-berlinite: In-

sights from density functional theory calculations, The Journal of Physical Chemistry C 124 (12) (2020) 6683–6688. doi:10.1021/acs.jpcc.9b11794.
URL https://pubs.acs.org/doi/10.1021/acs.jpcc.9b11794

[27] T. Duguet, A. Gavrielides, J. Esvan, T. Mineva, C. Lacaze-Dufaure, DFT simulation of XPS reveals Cu/epoxy polymer interfacial bonding, The Journal of Physical Chemistry C 123 (51) (2019) 30917–30925. doi:10.1021/acs.jpcc.9b07772.
URL https://pubs.acs.org/doi/full/10.1021/acs.jpcc.9b07772

[28] S. Li, Y. Zhao, H. Wan, J. Lin, J. Min, Molecular understanding of the interfacial interaction and corrosion resistance between epoxy adhesive and metallic oxides on galvanized steel, Materials 16 (8) (2023) 3061. doi:10.3390/ma16083061.
URL https://www.mdpi.com/1996-1944/16/8/3061

[29] Q. Tan, S. Pu, G. Zhu, C. Yin, G. Zhang, Z. Zhang, M. Wu, Y. Tan, F.-Q. Liu, A novel bonding strategy of hydrogel on titanium alloy for marine antifouling engineering: Multiple antifouling mechanisms and dft calculations, Journal of Alloys and Compounds 1010 (2025) 177508. doi:10.1016/j.jallcom.2024.177508.
URL https://www.sciencedirect.com/science/article/pii/S0925838824040969

[30] A. Iscen, N. C. Forero-Martinez, O. Valsson, K. Kremer, Acrylic paints: An atomistic view of polymer structure and effects of environmental pollutants, The Journal of Physical Chemistry B 125 (2021) 10854–10865.

doi:10.1021/acs.jpcb.1c05188.
URL https://pubs.acs.org/doi/10.1021/acs.jpcb.1c05188

[31] Y. Reyes-Mercado, F. Vázquez, F. J. Rodríguez-Gómez, Y. Duda, Effect of the acrylic acid content on the permeability and water uptake of poly(styrene-co-butyl acrylate) latex films, Colloid and Polymer Science 286 (5) (2008) 603–609. doi:10.1007/s00396-008-1838-6.
URL https://link.springer.com/article/10.1007/s00396-008-1838-6

[32] L. G. Aguiar, E. F. Souza, R. Giudici, Kinetic modeling of the copolymerization of acrylic acid and trimethylolpropane triacrylate over pre and post-gelation periods, European Polymer Journal 74 (2016) 264–278. doi:10.1016/j.eurpolymj.2015.11.033.
URL https://www.sciencedirect.com/science/article/pii/S0014305715300744

[33] P. Giannozzi, O. Baseggio, P. Bonfà, D. Brunato, R. Car, I. Carnimeo, C. Cavazzoni, S. de Gironcoli, P. Delugas, F. Ferrari Ruffino, A. Ferretti, N. Marzari, I. Timrov, A. Urru, S. Baroni, Quantum espresso toward the exascale, The Journal of Chemical Physics 152 (15) (2020) 154105. doi:10.1063/5.0005082.
URL https://pubs.aip.org/aip/jcp/article-abstract/152/15/154105/1058748/Quantum-ESPRESSO-toward-the-exascale

[34] J. P. Perdew, K. Burke, M. Ernzerhof, Generalized gradient approximation made simple, Phys. Rev. Lett. 77 (1996) 3865–3868. doi:

10.1103/PhysRevLett.77.3865.
URL https://link.aps.org/doi/10.1103/PhysRevLett.77.3865

[35] F. Birch, Finite elastic strain of cubic crystals, Phys. Rev. 71 (1947) 809–824. doi:10.1103/PhysRev.71.809.
URL https://link.aps.org/doi/10.1103/PhysRev.71.809

[36] H. J. Monkhorst, J. D. Pack, Special points for Brillouin-zone integrations, Physical Review B 13 (1976) 5188–5192. doi:10.1103/PhysRevB.13.5188.
URL https://link.aps.org/doi/10.1103/PhysRevB.13.5188

[37] M.-T. Nguyen, N. Seriani, R. Gebauer, Water adsorption and dissociation on (α-Fe_2O_3) (0001): PBE+U calculations, The Journal of Chemical Physics 138 (19) (2013) 194709. doi:10.1063/1.4804999.
URL https://pubs.aip.org/aip/jcp/article/138/19/194709/192327/Water-adsorption-and-dissociation-on-Fe2O3-0001

[38] R. B. Wang, A. Hellman, Initial water adsorption on hematite (α-Fe_2O_3) (0001): A DFT + U study, The Journal of Chemical Physics 148 (9) (2018) 094705. doi:10.1063/1.5020358.
URL https://pubs.aip.org/aip/jcp/article/148/9/094705/196817/Initial-water-adsorption-on-hematite-Fe2O3-0001-A

[39] J. D. Kubicki, K. W. Paul, D. L. Sparks, Periodic density functional theory calculations of bulk and the (010) surface of goethite, Geochemical Transactions 9 (1) (2008) 4. doi:10.1186/1467-4866-9-4.

URL https://geochemicaltransactions.biomedcentral.com/articles/10.1186/1467-4866-9-4

[40] E. Pedretti, P. Restuccia, M. C. Righi, Xsorb: A software for identifying the most stable adsorption configuration and energy of a molecule on a crystal surface, Computer Physics Communications 291 (2023) 108827. doi:10.1016/j.cpc.2023.108827.
URL https://www.sciencedirect.com/science/article/pii/S0010465523001728

[41] A. H. Larsen, J. J. Mortensen, J. Blomqvist, I. E. Castelli, R. Christensen, M. Dułak, J. Friis, M. N. Groves, B. Hammer, C. Hargus, E. D. Hermes, P. C. Jennings, P. B. Jensen, J. Kermode, J. R. Kitchin, E. L. Kolsbjerg, J. Kubal, K. Kaasbjerg, S. Lysgaard, J. B. Maronsson, T. Maxson, T. Olsen, L. Pastewka, A. Peterson, C. Rostgaard, J. Schiøtz, O. Schütt, M. Strange, K. S. Thygesen, T. Vegge, L. Vilhelmsen, M. Walter, Z. Zeng, K. W. Jacobsen, The atomic simulation environment—a python library for working with atoms, Journal of Physics: Condensed Matter 29 (27) (2017) 273002. doi:10.1088/1361-648X/aa680e.
URL https://iopscience.iop.org/article/10.1088/1361-648X/aa680e

[42] S. P. Ong, W. D. Richards, A. Jain, G. Hautier, M. Kocher, S. Cholia, D. Gunter, V. L. Chevrier, K. A. Persson, G. Ceder, Python Materials Genomics (pymatgen): A robust, open-source python library for materials analysis, Computational Materials Science 68 (2013) 314–319.

doi:10.1016/j.commatsci.2012.10.028.
URL https://linkinghub.elsevier.com/retrieve/pii/S0927025612006295

[43] H. T. T. Ta, N. V. Tran, M. C. Righi, Atomistic wear mechanisms in diamond: Effects of surface orientation, stress, and interaction with adsorbed molecules, Langmuir 39 (40) (2023) 14396–14403. doi:10.1021/acs.langmuir.3c01800.
URL https://pubs.acs.org/doi/10.1021/acs.langmuir.3c01800

[44] W. Knapp, D. Djomani, J.-F. Coulon, R. Grunchec, Influence of structuring by laser and plasma torch on the adhesion of metallic films on thermoplastic substrates, Physics Procedia 56 (2014) 791–800. doi:10.1016/j.phpro.2014.08.087.

[45] N. Issaoui, H. Ghalla, F. Bardak, M. Karabacak, N. Aouled Dlala, H. Flakus, B. Oujia, Combined experimental and theoretical studies on the molecular structures, spectroscopy, and inhibitor activity of 3-(2-thienyl)a-crylic acid through AIM, NBO,FT-IR, FT-Raman, UV and HOMO-LUMO analyses, and molecular docking, Journal of Molecular Structure 1130 (2017) 659–668. doi:10.1016/j.molstruc.2016.11.019.
URL https://www.sciencedirect.com/science/article/pii/S0022286016311759

[46] H.-F. Wang, Z.-P. Liu, Formic acid oxidation at pt/h2o interface from periodic dft calculations integrated with a continuum solvation model, The Journal of Physical Chemistry C 113 (40) (2009) 17502–17508. doi:

10.1021/jp9059888.
URL https://pubs.acs.org/doi/10.1021/jp9059888

[47] L. Guo, S. Kaya, I. B. Obot, X. Zheng, Y. Qiang, Toward understanding the anticorrosive mechanism of some thiourea derivatives for carbon steel corrosion: A combined dft and molecular dynamics investigation, Journal of Colloid and Interface Science 506 (2017) 478–485. doi:10.1016/j.jcis.2017.07.082.
URL https://www.sciencedirect.com/science/article/pii/S0021979717308494

[48] S. Peeters, C. Charrin, I. Duron, S. Loehlé, B. Thiebaut, M. C. Righi, Importance of the catalytic effect of the substrate in the functionality of lubricant additives: the case of molybdenum dithiocarbamates, Materials Today Chemistry 21 (2021) 100487. doi:10.1016/j.mtchem.2021.100487.
URL https://www.sciencedirect.com/science/article/pii/S2468519421000677

[49] F. Benini, P. Restuccia, M. C. Righi, Zinc dialkyldithiophosphates adsorption and dissociation on ferrous substrates: An ab initio study, Applied Surface Science 642 (2024) 158419. doi:10.1016/j.apsusc.2023.158419.
URL https://www.sciencedirect.com/science/article/pii/S0169433223020998

[50] S. Li, M. Zhang, Y. Dong, J. Gao, P. Cheng, H. Wang, Density functional theory study of P-doped Co_3O_4(111) facets for HCHO adsorption: Im-

plications for metal oxide semiconductor gas sensors, ACS Applied Nano Materials 6 (19) (2023) 17501–17511. doi:10.1021/acsanm.3c02656.
URL https://doi.org/10.1021/acsanm.3c02656

[51] C. Gattinoni, J. P. Ewen, D. Dini, Adsorption of surfactants on α-Fe_2O_3(0001): A density functional theory study, The Journal of Physical Chemistry C 122 (36) (2018) 20817–20826. doi:10.1021/acs.jpcc.8b05899.
URL https://pubs.acs.org/doi/full/10.1021/acs.jpcc.8b05899

[52] I. V. Chernyshova, S. Ponnurangam, P. Somasundaran, Adsorption of fatty acids on iron (hydr)oxides from aqueous solutions, Langmuir 27 (16) (2011) 10007–10018. doi:10.1021/la2017374.
URL https://pubs.acs.org/doi/full/10.1021/la2017374

[53] J. A. von Fraunhofer, Adhesion and cohesion, International Journal of Dentistry 2012 (1) (2012) 951324. doi:10.1155/2012/951324.
URL https://onlinelibrary.wiley.com/doi/abs/10.1155/2012/951324

[54] H. Zhu, Z. Guo, W. Liu, Adhesion behaviors on superhydrophobic surfaces, Chemical Communications 50 (2014) 3900–3913. doi:10.1039/C3CC47818A.
URL http://dx.doi.org/10.1039/C3CC47818A

[55] S. Ebnesajjad, Chapter 5 - theories of adhesion, in: S. Ebnesajjad (Ed.), Surface Treatment of Materials for Adhesive Bonding (Second Edition), second edition Edition, William Andrew Publishing, Oxford,

2014, pp. 77–91. doi:10.1016/B978-0-323-26435-8.00005-8.
URL https://www.sciencedirect.com/science/article/pii/B9780323264358000058

[56] M. Králik, Adsorption, chemisorption, and catalysis, Chemical Papers 68 (12) (2014) 1625–1638. doi:10.2478/s11696-014-0624-9.
URL https://link.springer.com/article/10.2478/s11696-014-0624-9

[57] A. Vinçotte, E. Beauvoit, N. Boyard, E. Guilminot, Effect of solvent on PARALOID® B72 and B44 acrylic resins used as adhesives in conservation, Heritage Science 7 (1) (2019) 42. doi:10.1186/s40494-019-0283-9.
URL https://www.nature.com/articles/s40494-019-0283-9

[58] E. Y. Lin, A. L. Frischknecht, K. I. Winey, R. A. Riggleman, Effect of surface properties and polymer chain length on polymer adsorption in solution, The Journal of Chemical Physics 155 (3) (2021) 034701. doi:10.1063/5.0052121.
URL https://pubs.aip.org/aip/jcp/article-abstract/155/3/034701/200712/Effect-of-surface-properties-and-polymer-chain

[59] L. I. Klushin, A. A. Polotsky, H.-P. Hsu, D. A. Markelov, K. Binder, A. M. Skvortsov, Adsorption of a single polymer chain on a surface: Effects of the potential range, Physical Review E 87 (2013) 022604. doi:10.1103/PhysRevE.87.022604.
URL https://link.aps.org/doi/10.1103/PhysRevE.87.022604

[60] E. Mete, M. Yortanlı, M. F. Danışman, A van der Waals DFT study of chain length dependence of alkanethiol adsorption on Au(111): physisorption vs. chemisorption, Physical Chemistry Chemical Physics 19 (2017) 13756–13766. doi:10.1039/C7CP01653K.
URL https://pubs.rsc.org/en/content/articlelanding/2017/cp/c7cp01653k

[61] M. Mu, F. A. Leermakers, J. Chen, M. Holmes, R. Ettelaie, Effect of polymer architecture on the adsorption behaviour of amphiphilic copolymers: A theoretical study, Journal of Colloid and Interface Science 644 (2023) 333–345. doi:10.1016/j.jcis.2023.04.051.
URL https://www.sciencedirect.com/science/article/pii/S0021979723006343

[62] F. P. Bowden, D. Tabor, The Friction and Lubrication of Solids, Oxford University Press, 1950. doi:10.1093/oso/9780198507772.001.0001.
URL https://global.oup.com/academic/product/the-friction-and-lubrication-of-solids-9780198507772